Near-Neutral-Colored Semitransparent Perovskite Films Using a Combination of Colloidal Self-Assembly and Plasma Etching

Lijing Zhang,[a,b] *Maximilian T. Hörantner,*[c] *Wei Zhang,*[c,d] *Qingfeng Yan,*[b,*] *Henry J. Snaith*[c,*]

[a]School of Chemistry, Dalian University of Technology, Dalian, Liaoning, P. R. China.

[b]Department of Chemistry, Tsinghua University, Beijing 100084, China

[c]Department of Physics, University of Oxford, Clarendon Laboratory, Parks Road, Oxford, OX1 3PU, UK

[d]School of Chemistry, University of Lincoln, Joseph Banks Laboratories, Beevor Street, Lincoln LN6 7DL, UK

Corresponding Author

Prof. Q. Yan

E-mail: yanqf@mail.tsinghua.edu.cn .

Prof. H. J. Snaith
E-mail: h.snaith1@physics.ox.ac.uk

Abstract

Organo-lead-halide perovskite based solar cells have achieved remarkable advancements in power conversion efficiencies (PCEs) in recent years. Given their attractive properties, possible applications for perovskites are wide ranging and among others, particularly appealing for building integrated photovoltaics (BIPVs). In this study, patterned perovskite films were successfully fabricated based on a microsphere lithography SiO_2 honeycomb scaffold template, which was derived by a combination of air-water interface self-assembly and O_2 plasma etching. These patterned perovskite films exhibited near-neutral-color and tunable semitransparency, which meet the requisites of semitransparent solar cells for BIPVs application. O_2 plasma etching of the microsphere template could effectively improve the active layer average visible transmission (AVT), and the existence of the SiO_2 nanoscaffold effectively smoothed the internal trade-off of active layer AVT and device PCE. Solar cell devices fabricated with these optimized patterened perovskite films yielded a maximum PCE of 10.3% with relatively high active layer AVT of 38%. This nanoscaffold patterned perovskite opens up a new strategy for design and fabrication of functional photoelectric device based on organo-lead-halide perovskite.

Keywords: Semi-transparent, Perovskite films, Solar Cell, Colloidal Crystal, Nanoscaffold

1. Introduction

Organic-inorganic lead halide perovskite based solar cells (PSCs) have received increasing interests over the past three years due to their high power conversion efficiencies (PCE), easy fabrication and low cost. The semiconducting perovskite materials demonstrated superior optoelectronic properties such as a high light absorption coefficient, a direct bandgap, large charge-carrier mobility and long diffusion length [1-3]. Since the first attempt reported by Miyasaka in 2009, the PCE of PSCs has boosted from an initial 3.8% to a recently certified 21% [4-9]. This rapid growth of PSCs research and the concurrent improvement in device performance enable other potential applications in the field of photovoltaics, e.g. wearable power source, portable electronic charges and building integrated photovoltaics (BIPVs) [10-13]. As a typical application of BIPVs, the neutral-colored semitransparent solar cells are commercially desired, which can integrate with the existing infrastructures such as building facades or windows to generate electricity and increase the aesthetic merits of the building.

Semitransparent perovskite solar cells are always achieved by combining semitransparent perovskite films together with transparent or semitransparent electrode [14-16]. Among which, the transparency of perovskite films plays a dominant role. As is known, the perovskite film on one hand absorbs light and converts the solar energy to electrical power. On the other hand, the high absorption coefficient of perovskite decreases the transparency of the film. There is an obvious trade-off between transparency and light absorbing in the photoactive layer, required

for generating power. To achieve good optical transmittance of the perovskite layer, two promising strategies to manipulate perovskite layers have been reported. Either reduce the thickness of perovskite film [16-19] or reduce perovskite coverage by microstructure formation [20-22]. The big challenge for the development of semitransparent devices is to prevent the direct electronic contact between the electron-transporting and hole-transporting materials. Such contact induces a shunting path for charges, which in turn decreases the performance, mostly visible in reducing the open-circuit voltage (V_{oc}) and fill factor (FF). The transparency can be improved efficiently by control of the perovskite layer thickness. For instance, You et al. [16] reported the semitransparent perovskite layer thickness varying from 350 nm to 150 nm fabricated by a one-step route. The average visible transmittance (AVT) increased from 5.84% to 21.76% while the corresponding solar cells' PCE decreased from 12.05% to 5.98%. The deterioration of the PCE was mostly due to the drop in V_{oc} as the perovskite layer became thinner and probably led to pinhole formation and therefore shunting paths. Other research groups have also observed similar decreases in V_{oc} based on similar solution processing methods [23,24]. Thermal co-evaporation has also been used to fabricate film solar cells [25]. Roldan et al. [12] prepared semitransparent perovskite films with thickness finely controlled from 280 nm to 40 nm by thermal co-evaporation. These films' AVT demonstrated a variation from 19% to 45%, while the PCE of corresponding solar cells changed from 7.73% to 3.39%. Similar results can be recognized in other literature [26,27]. However, it should be noted that it is technically not feasible to achieve high PCE and good AVT

simultaneously by only thinning the perovskite layer, as pinholes formation becomes unavoidable [28,29]. Moreover, because of the intrinsic absorption feature of the perovskite, the device will show orange red or brown yellow tint, which is not the most desirable option for the semitransparent PSC application. Fortunately, implementation of microstructure provides another strategy to achieve semitransparent devices. Eperon et al. reported neutral colored semitransparent PSCs based on perovskite microscale "islands" structure on desired substrates [20,21]. The AVT of the perovskite layer could be controlled from 7.2% to 60.3% with neutral color. However, the PCE of the device (≈ 6% at 20% AVT) was much lower than that of a typical perovskite solar cell with continuous thin film, even accounting for the lower levels of light absorption. The presence of regions between the perovskite islands provided the direct contact pathway for the p-type and n-type charge collection materials, leading to the formation of a "shunt diode", and lowering the V_{oc} drastically [20,21]. Selectively attaching molecular layers were introduced to counteract the performance loss through blocking the shunting-paths [30]. Recently, Hörantner et al. [22] developed a templating approach to introduce a periodic honeycomb structure into the perovskite thin film. The honeycomb region was predominantly transparent, whereas the perovskite domains within the honeycomb were strongly absorbing. As a result, semitransparent perovskite films with an active layer AVT of around 37% and red-brown color were obtained. Impressively, the incorporation of honeycomb scaffold led to an increase in both V_{oc} and FF for the devices and an average PCE of 7.9% were obtained. The patterned perovskite film via micro-templating technique opens a new

avenue to the optical enhancement. Based on this strategy, high transparency could be achieved by further increasing the proportion of honeycomb region over the total area of the substrate. However, the quantitative control of the coverage of honeycomb region for microstructural perovskite solar cells has not been reported and better balance between active layer AVT and device PCE need to be improved.

In this work, we present the fabrication of SiO_2 honeycomb (SiO_2 HC) structure for the patterning of perovskite films, with tuneable surface area coverage achieved by a combination of a highly reproducible colloidal monolayer (CM) templating and O_2 plasma etching. Colloidal self-assembly at the air/water interface has been regarded as a cost-effective method for quickly fabricating large-area monolayer colloidal crystals with enhanced quality and controllability [31,32]. O_2 plasma etching offers precise etching rates and removes the polystyrene (PS) shell in a layer-by-layer manner [33]. Thus, fine size control of the PS cores can be obtained by control the time of etching. We use the resultant PS cores array template to fabricate SiO_2 HC microstructures with varying coverage, which depends on the diameter of microspheres employed and the etching time. With subsequent spin coating and infiltration of the perovskite precursor solution, we obtain precise control of the SiO_2 HC structure patterned perovskite layer. By optimizing the microsphere diameter, O_2 plasma etching time and the concentration of precursor solution, we demonstrate near-neutral-colored semitransparent perovskite film with about 38 % active layer AVT. Solar cells based on these perovskite films achieved a PCE as high as 10.3 % and a high V_{oc} of 0.98 V.

2. Experiment

2.1 Substrate preparation.

The substrates used in this work was FTO-coated glass (Pilkington, 15 ohm/□). Initially, FTO was removed from regions under the anode contact by etching the FTO with 2M HCl and zinc powder. Substrates were then cleaned sequentially in 2% Hellmanex detergent, DI water, acetone, isopropanol and ethanol. A 10 min O_2 plasma etching was applied before the TiO_2 compact layer (c-TiO_2) was deposited by spin-coating a solution of 0.71 g titanium isopropoxide and 0.07 g HCl in 8 mL of ethanol. Then it was sintered on a hot plate up to 500 °C for 30 min. Spin-coating was carried out at 2,000 rpm for 60 s.

2.2 Preparation of PS colloidal monolayers and O_2 plasma etching.

Monodisperse PS colloidal spheres with a polydispersity less than 3% were synthesized using the emulsifier-free emulsion polymerization method [34,35]. The PS colloidal monolayer (CM) was prepared by using the air-water interface self-assembly method as reported in our previous work [32]. After diluted with equal volume of ethanol, the PS emulsion was dropped onto a small glass slide (1 cm×1 cm) which was placed in the center of a glass Petri dish (Φ = 12 cm) with top surface in the same level of water. During the spreading process, PS spheres spread rapidly to the water surface and assembled into 2D monolayer colloidal crystal arrays in several seconds. By controlling the drop volume (~ 200 μL) of colloidal suspension, large-area hexagonal close-packed CM covering the whole glass Petri dish was attained.

To transfer the CM to FTO/c-TiO_2 substrate, the liquid level was raised to almost the height of the Petri dish by adding more DI water. A FTO/c-TiO_2 substrate was

inserted beneath the CM and then lifted off from the water surface. Finally the PS CM was transferred to the substrate. After drying at room temperature, the substrate with PS CM was transferred to O_2 plasma reactor chamber (Diener Electronic, German). The O_2 plasma etching was performed under an excitation frequency of 13.56 MHz, a power of 100 W, a pressure of 2 Pa and a gas flow of 20 sccm. The etching degree is proportional to the etching time.

2.3 Fabrication of inversed SiO_2 honeycomb scaffold.

The SiO_2 honeycomb was fabricated by spin-coating a solution of 20 nm pre-made SiO_2 particles in ethanol [36] onto the PS or PS core monolayers. Subsequently the monolayer was sintered in multiple steps, i.e. drying at 100 °C for 15 min, quickly heated to 350 °C and held for 30 minutes to degrade polystyrene, then increased to 500 °C and sintered for 30 minutes to form a stable oxide honeycomb structure.

2.4 Perovskite deposition.

The perovskite solution was prepared by dissolving CH_3NH_3I and PbI_2 in anhydrous N, N-Dimethylformamide (DMF) at a 3:1 molar ratio with final concentrations of 10 wt%~40 wt%. Filling the honeycombs with perovskite was realized via spin-coating different concentrations (10 wt%~40 wt% in DMF) of $CH_3NH_3PbI_3$ [6] onto the patterned substrates. This was carried out in a N_2 filled glove box at a spin speed of 4000 rpm for 45 seconds. The perovskite layer was then annealed for 1.5 hours at 100 °C.

2.5 Perovskite solar cells preparation.

The hole-transporting layer spiro-OMeTAD (2,2',7,7'-tetrakis-(N,N-di-p-methoxyphenylamine)9,9'-spirobifluorene) was then deposited from a 66 mM chlorobenzene solution containing additives of lithium bis(trifluoromethanesulfonyl)imide and 4-tert-butylpyridine. The sample was dried overnight in a light-sealed desiccator. Finally, 120-nm-silver electrodes were thermally evaporated as the top-electrode under vacuum of ~10^{-6} Torr, at a rate of ~0.1 nm s^{-1}.

2.6 Characterization.

Morphologies of the PS and PS core arrays and the honeycomb patterned perovskite layer were observed by field-emission scanning electron microscope (FESEM, Gemini LEO 1530). The transmission measurements were carried out with an internally coupled integrated sphere in a UV-visible spectrophotometer (Varian Cary 300). To characterize the performance of the solar cells, J–V curves were measured (2400 Series SourceMeter, Keithley Instruments) under simulated AM 1.5 sunlight at 100 $mWcm^{-2}$ irradiance generated by an Abet Class AAB sun 2000 simulator, with the intensity calibrated with an NREL-calibrated KG5-filtered Si reference cell [37]. The mismatch factor was calculated to be less than 1%. The solar cells were masked with a metal aperture to define the active area, typically 0.0625 cm^2 (measured individually for each mask) and measured in a light-tight sample holder to minimize any edge effects and ensure that the reference cell and test cell were located in the same spot under the solar simulator during measurement.

3. Results and discussion

3.1 Fabrication and morphological studies.

Fig. 1 shows a schematic illustration of the fabrication process for SiO_2 HC structure patterned perovskite layer. Initially, a large-scale CM was prepared by the self-assembly of PS spheres at the air-water interface (Fig. 1a). It was then transferred onto the FTO/c-TiO_2 coated substrate and dried at room temperature (Fig. 1b). Subsequently, the substrate covered with PS CM was treated by a commercial oxygen plasma system to etch the PS spheres down to a desired diameter while conserving their position as well as spherical shape. In this way, a non-close packed hexagonally ordered primary "mask" was obtained (Fig. 1c). Then the SiO_2 nanoparticle solution was filled in the interstices between PS spheres via spin-coating (see Fig. 1d). After sintering to remove the PS CM template, the porous honeycomb structure was formed (Fig. 1e). Finally, the perovskite precursor solution was spin-coated onto the substrate with patterned SiO_2 HC structure and annealed at 100 ºC for 1.5 hours, resulting in a final SiO_2 HC structure patterned perovskite layer (Fig. 1f).

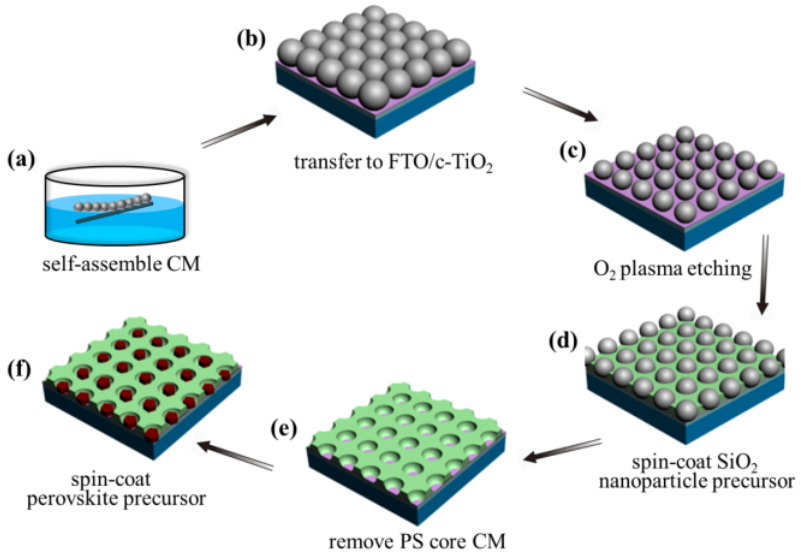

Fig. 1 Fabrication process for SiO_2 HC structure patterned perovskite layer. (a) Large-scale PS CM was prepared by self-assembly at the air–water interface. (b) PS monolayer was transferred onto the FTO/c-TiO_2 substrate. (c) A non-close packed hexagonally ordered PS core monolayer after O_2 plasma etching treatment. (d) Spin-coating of SiO_2 nanoparticles precursor solution to fill the gaps of the monolayer. (e) Inversed SiO_2 HC structure formed after sintering procedure. (f) SiO_2 HC structure patterned perovskite layer by spin-coating and followed by annealing treatment.

Based on this method, the corresponding SEM images of the samples of each step during the fabrication of the SiO_2 HC structure patterned perovskite layer are shown in Fig. 2a-2d. Fig. 2a demonstrates a well-arranged hexagonally close-packed 600 nm PS CM with few defects, which benefits from the mature self-assembly method [32,38,39]. Compared with Fig. 2a, it can be clearly observed that the diameter of PS spheres after O_2 plasma etching has shrunk to a smaller dimension from 600 nm to around 345 nm as shown in Fig. 2b, while conserving their position and spherical

shape. Fig. 2c shows the SiO_2 HC structure fabricated from the resultant 345 nm PS core template. It is worth noting that before filling the SiO_2 nanoparticles, the PS core template should be annealed at 105℃ for 15 min to ensure the bottom of the PS cores coalesce with the FTO/c-TiO_2 substrate and achieve a close contact between the perovskite domains and c-TiO_2 layer in the subsequent steps. After the two templating procedures, the perovskite domain eventually occupied the position of PS spheres and the transparent SiO_2 HC took over the interstice area (see Fig. 2d). The coverage of SiO_2 HC is theoretically determined by the original and residual PS. While, in a certain operating conditions, the residual PS size was mainly determined by O_2 plasma etching time, thus the proportion of inverse-honeycomb region could be tuned by controlling the etching time. The detail analysis may refer the discussion in Fig. S1 in the supporting information. In Fig. 2e, g, i we present another three PS spheres with original diameter of 400 nm, 1.0 μm and 1.5 μm after etching for 5, 10 and 20 min, respectively, as well as their corresponding inversed SiO_2 HC scaffolds (Fig. 2f, h, j). The matrix of various original PS CMs with different etching time is demonstrated in detail in Fig. S2 in the supporting information.

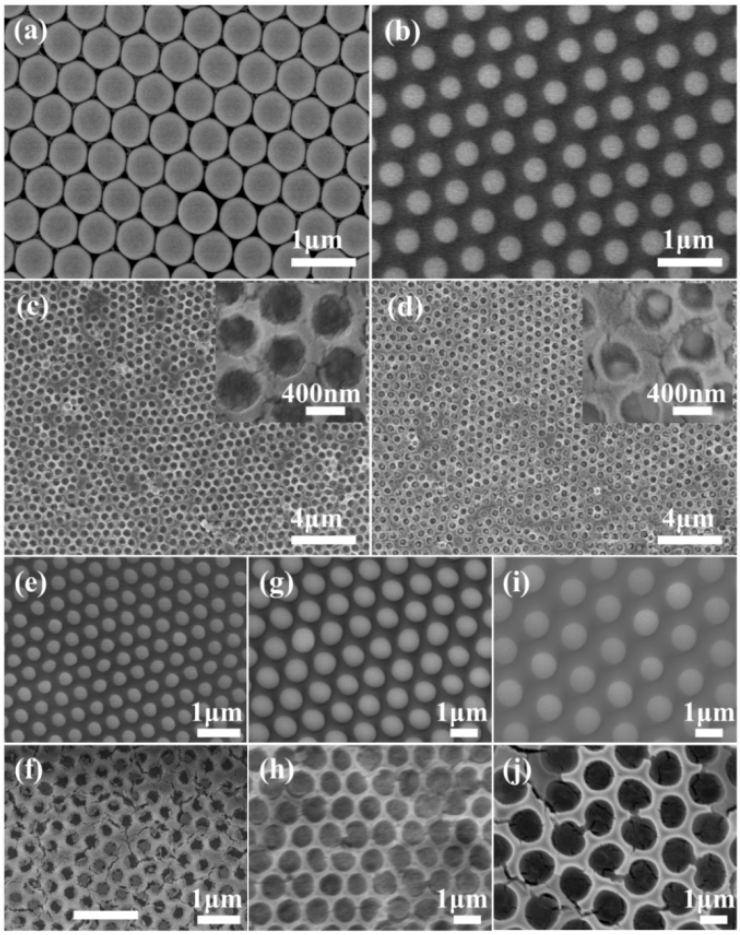

Fig. 2 SEM images of (a) A 600 nm PS CM transferred onto a FTO/c-TiO_2 substrate. (b) Non-close packed hexagonally ordered PS array after O_2 plasma etching for 8 min. (c) SiO_2 HC structure fabricated from the template shown in (b). (d) SiO_2 HC structure patterned perovskite layer prepared by spin-coating of a 20 wt% perovskite precursor solution. SEM images show PS core CMs and corresponding inversed SiO_2 HC structure based on different PS sphere diameters and different O_2 plasma etching time. (e, f) 420 nm-5 min, (g, h) 1.0 μm-15 min and (i, j) 1.5 μm-20 min.

3.2 Transmittance and photovoltaic performance.

In order to characterize such films for their use in working solar cells, the optical behavior of not just the perovskite but the whole active layer necessary to produce a working solar cell should be studied. Following the method described by Eperon et al.,

we define the active layer of fabricated perovskite films as the structure of c-TiO_2/SiO_2 HC patterned perovskite/spiro-OMeTAD. The active layer transmittance can be calculated following an approximate formula [20],

$$T_{AL} = \frac{T_{FTO+AL}}{T_{FTO}} \quad (1)$$

the T_{FTO+AL} and T_{FTO} can be measured directly with a UV-visible spectrophotometer, AL stands for the active layer. Furthermore, as the application of semitransparent perovskite films is for visible aesthetics, we are interested in the visible wavelengths between 400 and 750 nm, and the AVT of active layer is the mean transmittance between these wavelengths.

3.2.1 E□ect of the O_2 plasma etching time.

The etching time of a PS CM template plays an important role in determining the coverage ratio of SiO_2 HC to perovskite domains, and finally affects the active layer transparency and performance of PSCs. Taking the 600 nm PS CM as an example, the effect of etching time on the transparency of the active layer and the corresponding device performance was studied by changing the etching time while fixing the perovskite precursor solution as 30 wt%.

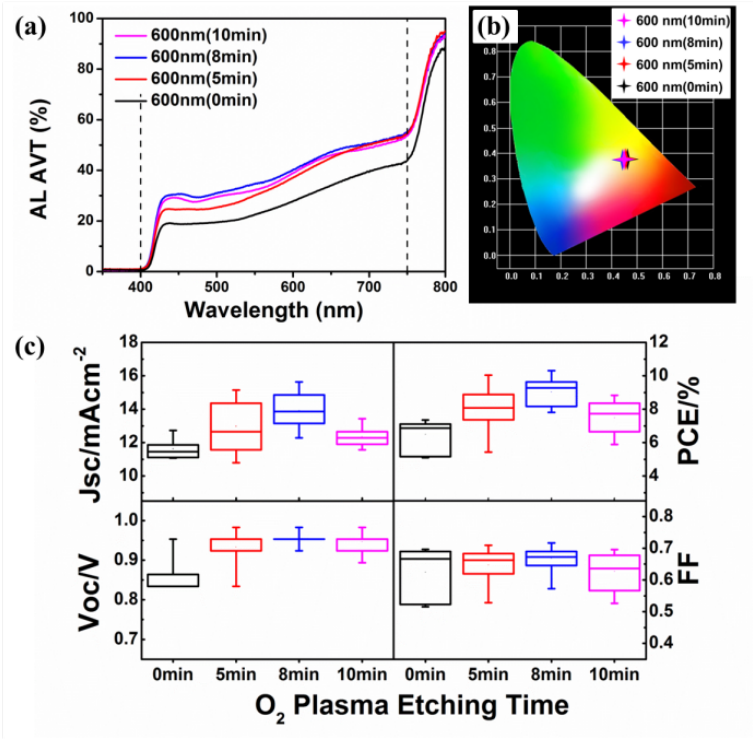

Fig. 3 (a) Transmittance spectra of active layers of perovskite films fabricated from the 600 nm CMs after O_2 plasma treatment for 0, 5, 8 and 10 min, measured with an integrating sphere. (b) Color coordinates of the semitransparent perovskite films with transmittance spectra shown in (a) on the CIE xy chromaticity diagram. (c) Box-plot of the device performance for the solar cells based on corresponding perovskite films.

Fig. 3a shows the transmission spectra of active layers of representative patterned perovskite films. As seen from Fig. 3a, the near-flat spectra across the majority of the visible spectrum are presented. As expected, the transmittance increases with increasing the plasma etching time of 600 nm PS CMs at the initial etching stage (e.g. 0 to 8 min) and slightly declines when the etching time reached 10 min. The decline is probably due to the over small residual PS cores caused by over etching (see Fig. S3 in the supporting information) and capping layer of perovskite formation during the

process of perovskite spin coating. The film fabricated from the CM etched for 8 min (600 nm-8 min) presents the best AL AVT about 38 % and an increase by 42 % is achieved as compared with the one without O_2 plasma treatment. In this regard, increasing the interstice area between adjacent PS spheres by O_2 plasma etching can greatly improve the active layer transmittance and lay the foundation for developing semitransparent working devices. To quantify the color-neutrality of the active layers, we calculated x and y color parameters for the samples according to their transmission spectra of the active layer in question and displayed the results on the CIE 1931 xy chromacity diagram in Fig. 3b. The reference daylight illuminant D65 was also presented. The color coordinates of these patterned semitransparent active layers are located nearly the same position and close to the daylight D65 reference, representing excellent color-neutrality.

In Fig. 3c we present the performance of the solar cells based on these patterned perovskite films. As can be seen by the reasonable device performances, all the solar cells operate well, indicating a good contact between the FTO/c-TiO_2 substrate and the perovskite layer within the SiO_2 pores. The short circuit current density (J_{sc}) monotonically increases with the increase of the etching time before over etching (10 min). Meanwhile, the V_{oc} and FF display the same trend. We also observe that for cells based on etched templates, they all present high V_{oc} and FF compared with the one without etching. As a result, the PCEs of these devices also show the similar trend and the solar cell based on 600 nm-8 min patterned perovskite film exhibits the best

performance with an average current voltage measured PCE of 9.7 ± 0.4 %, showing good potential for making efficiently working devices.

Interestingly, we find that both-device PCE and active layer AVT increase with the etching time before over etched (10 min). As described in the introduction part, there is a reciprocal balance between PCE and AVT. However, because of the existence of the SiO_2 HC structure, the spatial environment for crystallization of perovskite have changed and affected the final performance of the perovskite films in both device PCE and active layer AVT. According to the analysis of Fig. S1 in the supporting information, the increase with the etching time, leading to the corresponding increase of active layer AVT (0 min to 8 min). For the PCE situation, the SiO_2 HC structure provides a confined space for perovskite crystals, which shrank gradually with the increase of etching time, and the curvature of "micro-bowls" will increase correspondingly. For the fixed amount of precursor solution, the thickness of each perovskite crystal in confined SiO_2 pores increased correspondingly, leading to the increase of V_{oc} and FF, as well as the PCE of these patterned perovskite film based solar cells. For the case of 10 min, the over etched PS cores only formed some shallow scallops, the thinner perovskite layer and pinholes led to the drop of PCE. In other words, the intrinsic trade-off between PCE and AVT can be smoothed by the patterned SiO_2 HC structure. The enhanced V_{oc} and FF can be explained by the existence of SiO_2 oxide [40]. The SiO_2 honeycomb structure acts as an insulating grid between the perovskite domains to prevent electronic contact between the hole transporting layer and the electron transporting layer. Through the prevention of these shunting paths that

usually arise between the perovskite "islands" the shunt resistance is increased, which usually has a positive effect on the FF and Voc in devices [41].This has also been described Eperon et al and Hörantner et al in much detail [21,22]. The key parameters for average performing of solar cells fabricated from 600 nm PS CMs etching for different time are summarized in Table 1.

Table. 1 Key parameters for average performing of perovskite films and corresponding solar cells based on 600 nm CMs etching for different time. AVT is average visible transmission of the whole perovskite films without top electrode; AL AVT is the active layer AVT, which excludes absorption losses in the FTO anode and the top electrode.

etching time (min)	AVT (%)	AL AVT (%)	J_{SC} (mA/cm^2)	V_{OC} (V)	FF (-)	PCE (%)
0	24	27	12.3±0.7	0.85±0.15	0.53±0.10	5.7±2.4
5	31	35	14.8±0.4	0.95±0.02	0.63±0.05	9.0±0.9
8	34	38	15.0±0.4	0.97±0.02	0.66±0.02	9.7±0.4
10	32	36	12.5±0.7	0.95±0.02	0.64±0.04	7.8±0.7

Similarly, the active layer AVT and device PCE value of patterned perovskite films fabricated from the PS CM templates of different original diameter (420 nm, 1 μm and 1.5 μm) and different etching time were also systematically studied. These results are shown in Fig. S4 in the supporting information, which demonstrates that the original 600 nm PS sphere is the optimal option under current conditions but all other

diameters show a similar trend in device PCE and active layer AVT for different etching times.

3.2.2 Effect of the perovskite precursor concentration

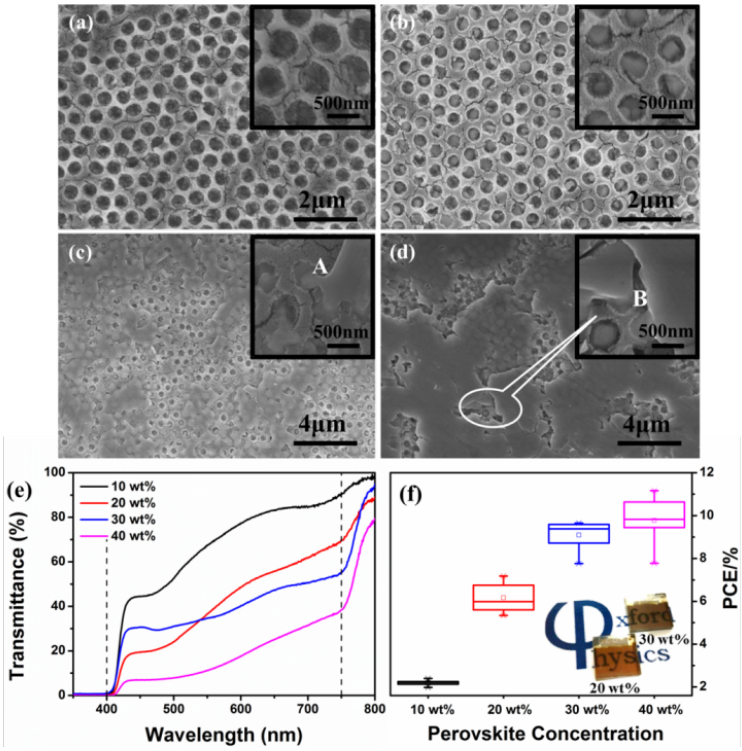

Fig. 4 SEM images (top view) showing perovskite film formation within SiO_2 HC scaffolds on FTO/c-TiO_2 substrate derived from 600 nm-8 min etching PS core CMs and infiltrated with different perovskite precursor concentration (a) 10 wt% (b) 20 wt% (c) 30 wt% and (d) 40 wt%. (e) Transmittance spectra of active layers of these perovskite films. (f) Box-plot of the PCE performance for the corresponding solar cell devices based on these perovskite films.

For a SiO_2 HC scaffold structure derived from PS CMs, the ability to template the perovskite materials is limited [17,27]. Here we investigate the influence of perovskite precursor concentration on the film morphology. Based on 600 nm-8 min etching PS

CMs, we fabricated SiO_2 HC scaffold patterned perovskite films with perovskite precursor concentrations varying from 10 wt% to 40 wt%. Fig. 4 a-d show the top view SEM images of corresponding perovskite film morphologies. The corresponding cross-sectional SEM images (supporting Information, Fig. S5) proposed the thickness of SiO_2 HC scaffold is about 200 nm. When the perovskite concentration is below 20 wt%, the perovskite films appear to be completely uniform, and show random formations of perovskite domains within SiO_2 HC scaffold. Since the existence of SiO_2 HC pores, the perovskite growth is limited by the honeycomb walls. This results in good filling behaviour within the pores and therefore presents patterned perovskite domains with controllable size and coverage. However, the honeycomb pores are significantly smaller than the randomly formed perovskite crystals when higher concentration precursor was filled, an additional capping layer will formed on top of SiO_2 HC scaffold (Fig. 4c and 4d), the thickness and coverage of capping layer will increase as the increase of concentration. For 40 wt% samples, the perovskite capping layer caps most of the surface of honeycomb region and present dark red color. Fig. 4e shows the active layer transmittance of these perovskite films infiltrated from different precursor concentration. The active layer AVT decreases dramatically from 66% to 17%，with the perovskite precursor concentration varying from 10 wt% to 40 wt%. It is noteworthy that for 20 wt% and 30 wt% concentrations, although the AL AVT is close, the spectrum line of 30 wt% presents a flatter spectrum over a broad range than 20 wt% films. As a result, the color of the 30 wt% film is much closer to neutral color, as displayed on the CIE xy chromacity diagram in Fig. S6 in the supporting

information. This means a random super thin capping layer may be have beneficial effects in improving the film's color-neutrality. The exact mechanism is not very clear and need to be studied further. The photographs of 20 wt% and 30 wt% films are shown in inset of Fig. 4f.

The PCE performance of solar cells made of different perovskite precursor concentration are also invested, as shown in Fig. 4f. With the increasing of the precursor concentration from 10 wt% to 40 wt%, the average PCE increases from 2.2% to 9.8%, which is mainly attributed to the enhanced light absorption with thickness increasing. Among which, the cells with 30 wt% perovskite film demonstrate significant improvement in PCE of 9.1% compared with these based on 20 wt% perovskite films with PCE only 6.2%. The improvement may be lies in the high V_{oc} and FF for the existence of thin capping layer. Considering the active layer AVT and cells PCE comprehensively, the patterned perovskite film with thin capping layer infiltrated from 30 wt% precursor concentration present excellent performance in future BIPV application. All the solar cells parameters are summarized in Table 2.

Table. 2 Key parameters for average performing of perovskite films and corresponding solar cells based on 600 nm-8 min CMs with different concentration of the perovskite precursor solution.

Conc. (wt%)	AVT (%)	AL AVT (%)	J_{SC} (mA/cm^2)	V_{OC} (V)	FF (-)	PCE (%)
10	59	66	4.0±0.3	0.86±0.02	0.65±0.04	2.2±0.13
20	36	40	11.9±1.9	0.89±0.09	0.53±0.07	6.2±0.65
30	34	38	16.5±0.5	0.98±0.02	0.56±0.04	9.1±0.70
40	15	17	17.5±1.3	0.98±0.02	0.56±0.05	9.8±1.06

3.2.3 Advantages of nanoscaffold strategy and champion solar cells performance

The comparison in active AVT and solar cells performance of semitransparent perovskite films fabricated from direct dewetting, solution processing and our SiO_2 HC scaffold (600 nm-8 min) strategy were shown in Fig. 5. The perovskite precursor concentration was fixed as 30 wt%. The dewetting method is to spin coat perovskite films directly on FTO/c-TiO_2 substrate, and microstructured arrays of perovskite "islands" will formed [20]. While the solution processing method is to fabricate perovskite films on a mesostructured layer of Al_2O_3 coated FTO/c-TiO_2 substrate, the transparency can be achieved by controlling the thickness of perovskite film via decrease the perovskite precursor concentration [6]. The provskite film fabricated from 30 wt% precursor solution only present 5.8% active layer AVT, much lower than dewetting and SiO_2 HC scaffold strategy. Thus 20 wt% precursor solution was chosen, and the fabricated film presents 29.6% active layer AVT. The SiO_2 HC scaffold patterned film presents similar active layer AVT of 38% compared with the dewetting film of 40% (Fig. 5a), and the two films show similar color coordinates on the CIE xy 1931 chromacity diagram, which is much closer to the daylight illuminant D65 compared with solution method films (Fig. 5b). Solar cells based on SiO_2 HC scaffold patterned perovskite films exhibit excellent PCE performance, which is similar to

solution ones (30 wt%) and much higher than dewetting ones. For the existence of insulated SiO_2 HC scaffold, the V_{oc} and FF were effectively enhanced by suppression of recombination, or avoiding the direct contact between the hole-blocking layer (c-TiO_2) and the hole-transporting layer (spiro-OMeTAD) [22,41]. Therefore, the SiO_2 HC scaffold strategy provide new venue for fabricate high-efficiency and neutral-colored semitransparent device for BIPV and other industrial semitransparent applications.

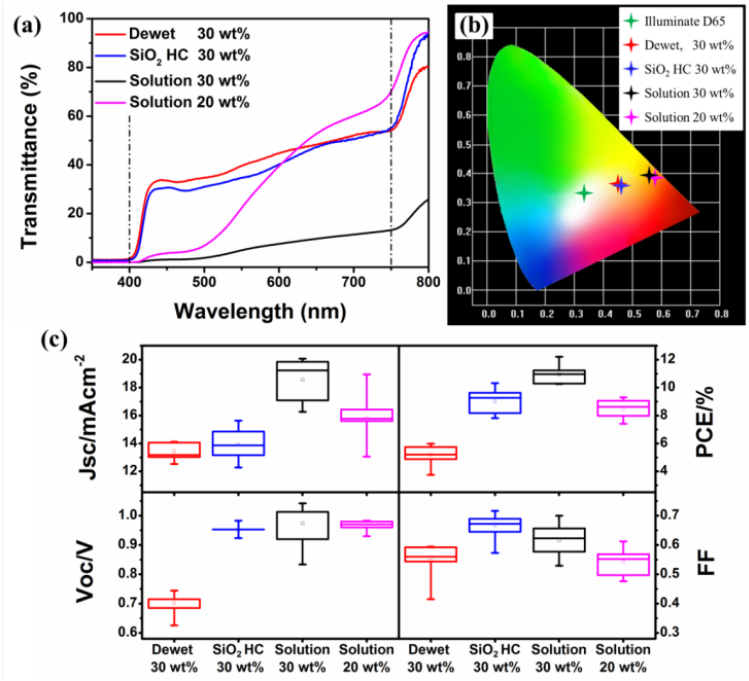

Fig. 5 (a) Transmittance spectra of active layers of perovskite films fabricated by dewetting, SiO_2 HC scaffold and solution method with precursor concentration as 30 wt% (or 20 wt%). (b) Color coordinates of the semitransparent perovskite films with transmittance spectra shown in (a) on the CIE xy chromaticity diagram. (c) Box-plot of the device performance for the corresponding solar cells based on perovskite films fabricated by these three methods.

Finally, we show in Fig. 6a the J-V curve for the champion solar cells fabricated by SiO_2 HC scaffold template from the 600 nm-8 min etching PS CM with 30 wt% perovskite precursor. When measured under simulated AM 1.5G (100 $mWcm^{-2}$) solar irradiation in air, the cells exhibited outstanding performance with J_{sc}= 15.6 $mAcm^{-2}$, V_{oc} = 0.98 V, FF = 0.66 and PCE = 10.3% when scanned from forward bias (FB) to short circuit (SC), and J_{sc}= 15.70 $mAcm^{-2}$, V_{oc} = 0.89 V, FF = 0.53 and PCE = 7.5% when scanned from SC to FB. The hysteresis between forward and backward J-V scan is due to a combination of the presence of mobile ions and electronic traps near the charge collection layers as has been recently elucidated [42-44]. The inset shows the photograph of this cell without top electrode which demonstrates near-neutral color and semitransparency. A reasonable method to compare cells that exhibit hysteresis is to measure the stabilized power output under load near the maximum power point over time. We recorded the photocurrent of this cell held at a forward bias of 0.71 V as a function of time to gain some understanding of the stabilized power output under working conditions (Fig. 6b). The photocurrent stabilizes within seconds to approximate 8.9 $mAcm^{-2}$, and yielding a stabilized PCE of 6.6% measured after 100 s. This is substantial, but indicates that further work should be done to improve the stabilized output of the solar cells, most likely achievable by using more suitable electron extraction layers, such as fullerene derivatives [45-47].

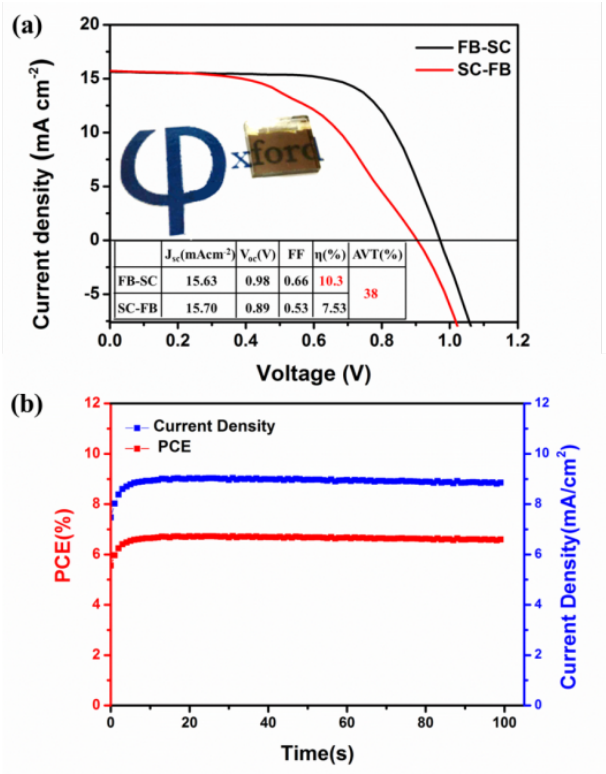

Fig. 6 (a) FB-SC and SC-FB J-V curves measured under AM1.5 simulated sun light with a scan rate of 0.15 Vs-1 for the best-performing PSC device based on the 600 nm-8 min etching CM with 30% perovskite precursor. The inset is the photograph of the same cell without top electrode which demonstrates neutral color and semitransparency. (b) Photocurrent density and PCE as a function of time for the same cell held at a forward bias of 0.71 V. The cell was placed in the dark prior to the start of the measurement.

4. Conclusions

In summary, we have presented an improved, scalable and reproducible technique for fabricating highly ordered SiO_2 HC scaffold patterned perovskite thin films. The SiO_2 HC scaffold structure could be finely controlled by PS sphere size chosen and O_2 plasma etching time. These patterned perovskite films exhibited near-neutral-color and

tunable semitransparency. Solar cells constructed with these patterned perovskite films exhibited respectable solar cell efficiency with enhanced V_{oc} and FF. O_2 plasma treatment effectively increased the photoactive layer AVT and device PCE at the same time. Solar cells fabricated from 600 nm-8 min etching PS CM with 30 wt% perovskite precursor yielded a maximum PCE of 10.3% with relatively high photoactive layer AVT of 38%. The present approach offers a new platform for the development of high-performance semitransparent solar cells when combined with transparent or semitransparent electrodes, which represents a major step forward for the practical application of semitransparent technology. Notably, effort is now required to apply this approach to device configurations (and n- and p-type material choices) which exhibit negligible current voltage hysteresis. The precise adjustability of the scaffold pores could lead to a perfectly tunable 2D geometry of perovskite arrays, interesting for optoelectronic applications such as 2D-distributed feedback lasers or light emitting diodes [48-51].

Acknowledgements

This work was supported by the EPSRC under the Supergen Super Solar hub, and the ERC StG2011 project Hyper. The authors also thank financial support from the National Science Foundation of China (Nos. 51173097, and 91333109) and the National Key Basic Research Program of China (No. 2013CB632900). The Tsinghua University Initiative Scientific Research Program (Nos. 20131089202, 20161080165) and the Open Research Fund Program of the State Key Laboratory of

Low-Dimensional Quantum Physics (No. KF201516) are acknowledged for partial financial support. The authors also thank Giles Eperon, Wenzhe Li, Jiandong Fan and Jacob Wang for fruitful discussions, and Jin Zhang for the preparation of SiO_2 nanoparticle solution and perovskite solution.

Appendix A. Supplementary material

Supplementary data associated with this article can be found in the online version at...

References

[1] A. Kojima, K. Teshima, Y. Shirai, T. Miyasaka, Organometal halide perovskites as visible-light sensitizers for photovoltaic cells, J. Am. Chem. Soc. 131 (2009) 6050-6051.

[2] S. Sun, T. Salim, N. Mathews, M. Duchamp, C. Boothroyd, G. Xing, T.C. Sum, Y.M. Lam, The origin of high efficiency in low-temperature solution-processable bilayer organometal halide hybrid solar cells, Energ. Environ. Sci. 7 (2014) 399-407.

[3] S.D. Stranks, G.E. Eperon, G. Grancini, C. Menelaou, M.J. Alcocer, T. Leijtens, L.M. Herz, A. Petrozza, H.J. Snaith, Electron-hole diffusion lengths exceeding 1 micrometer in an organometal trihalide perovskite absorber, Science 342 (2013) 341-344.

[4] National Renewable Energy Laboratory, Best Research-Cell Efficiencies chart; www.nrel.gov/ncpv/images/efficiency_chart.jpg.

[5] N.J. Jeon, J.H. Noh, Y.C. Kim, W.S. Yang, S. Ryu, S.I. Seok, Solvent engineering for high-performance inorganic–organic hybrid perovskite solar cells, Nat. Mater. 13 (2014) 897-903.

[6] M.M. Lee, J. Teuscher, T. Miyasaka, T.N. Murakami, H.J. Snaith, Efficient hybrid solar cells based on meso-superstructured organometal halide perovskites, Science 338 (2012) 643-647.

[7] W.S. Yang, J.H. Noh, N.J. Jeon, Y.C. Kim, S. Ryu, J. Seo, S.I. Seok, High-performance photovoltaic perovskite layers fabricated through intramolecular exchange, Science 348 (2015) 1234-1237.

[8] J. Burschka, N. Pellet, S.-J. Moon, R. Humphry-Baker, P. Gao, M.K. Nazeeruddin, M. Grätzel, Sequential deposition as a route to high-performance perovskite-sensitized solar cells, Nature 499 (2013) 316-319.

[9] H.-S. Kim, C.-R. Lee, J.-H. Im, K.-B. Lee, T. Moehl, A. Marchioro, S.-J. Moon, R. Humphry-Baker, J.-H. Yum, J.E. Moser, Lead iodide perovskite sensitized all-solid-state submicron thin film mesoscopic solar cell with efficiency exceeding 9%, Sci. Rep-UK. 2 (2012) 591.

[10] P. Du, X. Hu, C. Yi, H.C. Liu, P. Liu, H.L. Zhang, X. Gong, Self‐Powered Electronics by Integration of Flexible Solid‐State Graphene‐Based Supercapacitors with High Performance Perovskite Hybrid Solar Cells, Adv. Funct. Mater. 25 (2015) 2420-2427.

[11] J.-H. Im, I.-H. Jang, N. Pellet, M. Grätzel, N.-G. Park, Growth of CH3NH3PbI3 cuboids with controlled size for high-efficiency perovskite solar cells, Nat. Nanotechnol. 9 (2014) 927-932.

[12] C. Roldán-Carmona, O. Malinkiewicz, R. Betancur, G. Longo, C. Momblona, F. Jaramillo, L. Camacho, H.J. Bolink, High efficiency single-junction semitransparent perovskite solar cells, Energ. Environ. Sci. 7 (2014) 2968-2973.

[13] B.J. Kim, D.H. Kim, Y.-Y. Lee, H.-W. Shin, G.S. Han, J.S. Hong, K. Mahmood, T.K. Ahn, Y.-C. Joo, K.S. Hong, Highly efficient and bending durable perovskite solar cells: toward a wearable power source, Energ. Environ. Sci. 8 (2015) 916-921.

[14] F. Guo, H. Azimi, Y. Hou, T. Przybilla, M. Hu, C. Bronnbauer, S. Langner, E. Spiecker, K. Forberich, C.J. Brabec, High-performance semitransparent perovskite solar cells with solution-processed silver nanowires as top electrodes, Nanoscale 7 (2015) 1642-1649.

[15] Z. Liu, P. You, S. Liu, F. Yan, Neutral-color semitransparent organic solar cells with all-graphene electrodes, ACS nano 9 (2015) 12026-12034.

[16] P. You, Z. Liu, Q. Tai, S. Liu, F. Yan, Efficient semitransparent perovskite solar cells with graphene electrodes, Adv. Mater. 27 (2015) 3632-3638.

[17] E. Della Gaspera, Y. Peng, Q. Hou, L. Spiccia, U. Bach, J.J. Jasieniak, Y.-B. Cheng, Ultra-thin high efficiency semitransparent perovskite solar cells, Nano Energy 13 (2015) 249-257.

[18] J.W. Jung, C.C. Chueh, A.K.Y. Jen, High-performance semitransparent perovskite solar cells with 10% power conversion efficiency and 25% average visible transmittance based on transparent CuSCN as the hole-Transporting material, Adv. Energy Mater. 5 (2015) 1500486.

[19] S. Aharon, M. Layani, B.E. Cohen, E. Shukrun, S. Magdassi, L. Etgar, Self-assembly of perovskite for fabrication of semitransparent perovskite solar cells, Adv. Mater. Interfaces 2 (2015) 1500118.

[20] G.E. Eperon, V.M. Burlakov, A. Goriely, H.J. Snaith, Neutral color semitransparent microstructured perovskite solar cells, ACS nano 8 (2013) 591-598.

[21] G.E. Eperon, D. Bryant, J. Troughton, S.D. Stranks, M.B. Johnston, T. Watson, D.A. Worsley, H.J. Snaith, Efficient, Semitransparent neutral-colored solar cells based on microstructured formamidinium lead trihalide perovskite, J. Phys. Chem. Lett. 6 (2014) 129-138.

[22] M.T. Hörantner, W. Zhang, M. Saliba, K. Wojciechowski, H. Snaith, Templated microstructural growth of perovskite thin films via colloidal monolayer lithography, Energ. Environ. Sci. 8 (2015) 2041-2047.

[23] M. Xiao, F. Huang, W. Huang, Y. Dkhissi, Y. Zhu, J. Etheridge, A. Gray-Weale, U. Bach, Y.B. Cheng, L. Spiccia, A fast deposition-crystallization procedure for highly efficient lead iodide perovskite thin-film solar cells, Angew. Chem. 126 (2014) 10056-10061.

[24] J. Xiong, B. Yang, R. Wu, C. Cao, Y. Huang, C. Liu, Z. Hu, H. Huang, Y. Gao, J. Yang, Efficient and non-hysteresis $CH_3NH_3PbI_3$/PCBM planar heterojunction solar cells, Org. Electron. 24 (2015) 106-112.

[25] Z. Zang, A. Nakamura, J. Temmyo, Single cuprous oxide films synthesized by radical oxidation at low temperature for PV application, Opt. Express 21 (2013) 11448-11456

[26] A. Cannavale, G.E. Eperon, P. Cossari, A. Abate, H.J. Snaith, G. Gigli, Perovskite photovoltachromic cells for building integration, Energ. Environ. Sci. 8 (2015) 1578-1584.

[27] C.O.R. Quiroz, I. Levchuk, C. Bronnbauer, M. Salvador, K. Forberich, T. Heumüller, Y. Hou, P. Schweizer, E. Spiecker, C.J. Brabec, Pushing efficiency limits for semitransparent perovskite solar cells, J. Mater. Chem. A 3 (2015) 24071-24081.

[28] G.E. Eperon, V.M. Burlakov, P. Docampo, A. Goriely, H.J. Snaith, Morphological Control for High Performance, Solution‐Processed Planar Heterojunction Perovskite Solar Cells, Adv. Funct. Mater. 24 (2014) 151-157.

[29] P.W. Liang, C.Y. Liao, C.C. Chueh, F. Zuo, S.T. Williams, X.K. Xin, J. Lin, A.K.Y. Jen, Additive enhanced crystallization of solution‐processed perovskite for highly efficient planar‐heterojunction solar cells, Adv. Mater. 26 (2014) 3748-3754.

[30] M.T. Hörantner, P.K. Nayak, S. Mukhopadhyay, K. Wojciechowski, C. Beck, D. McMeekin, B. Kamino, G.E. Eperon, H.J. Snaith, Shunt‐Blocking Layers for Semitransparent Perovskite Solar Cells, Adv. Mater. Interfaces 3 (2016) 1500837.

[31] M. Retsch, Z. Zhou, S. Rivera, M. Kappl, X.S. Zhao, U. Jonas, Q. Li, Fabrication of Large‐Area, Transferable Colloidal Monolayers Utilizing Self‐Assembly at the Air/Water Interface, Macromo. Chem. Phys. 210 (2009) 230-241.

[32] J. Yu, Q. Yan, D. Shen, Co-self-assembly of binary colloidal crystals at the air–water interface, ACS Appl. Mater. Inter. 2 (2010) 1922-1926.

[33] A. Plettl, F. Enderle, M. Saitner, A. Manzke, C. Pfahler, S. Wiedemann, P. Ziemann, Non‐Close‐Packed Crystals from Self‐Assembled Polystyrene Spheres by

Isotropic Plasma Etching: Adding Flexibility to Colloid Lithography, Adv. Funct. Mater. 19 (2009) 3279-3284.

[34] S.E. Shim, Y.J. Cha, J.M. Byun, S. Choe, Size control of polystyrene beads by multistage seeded emulsion polymerization, J. Appl. Polym. Sci. 71 (1999) 2259-2269.

[35] X. Du, J. He, Facile size-controllable syntheses of highly monodisperse polystyrene nano-and microspheres by polyvinylpyrrolidone-mediated emulsifier-free emulsion polymerization, J. Appl. Polym. Sci. 108 (2008) 1755-1760.

[36] G. Bogush, M. Tracy, C. Zukoski, Preparation of monodisperse silica particles: control of size and mass fraction, J. Non-Cryst. Solids 104 (1988) 95-106.

[37] H.J. Snaith, How should you measure your excitonic solar cells?, Energ. Environ. Sci. 5 (2012) 6513-6520.

[38] J. Yu, C. Geng, L. Zheng, Z. Ma, T. Tan, X. Wang, Q. Yan, D. Shen, Preparation of high-quality colloidal mask for nanosphere lithography by a combination of air/water interface self-assembly and solvent vapor annealing, Langmuir 28 (2012) 12681-12689.

[39] C. Geng, L. Zheng, J. Yu, Q. Yan, T. Wei, X. Wang, D. Shen, Thermal annealing of colloidal monolayer at the air/water interface: a facile approach to transferrable colloidal masks with tunable interstice size for nanosphere lithography, J. Mater. Chem. 22 (2012) 22678-22685.

[40] S.H. Hwang, J. Roh, J. Lee, J. Ryu, J. Yun, J. Jang, Size-controlled $SiO2_2$ nanoparticles as scaffold layers in thin-film perovskite solar cells, J. Mater. Chem. A 2 (2014) 16429-16433.

[41] K. Bouzidi, M. Chegaar, A. Bouhemadou, Solar cells parameters evaluation considering the series and shunt resistance, Sol. Energ. Mat. Sol. C, 91 (2007) 1647-1651.

[42] S. van Reenen, M. Kemerink, H.J. Snaith, Modeling anomalous hysteresis in perovskite solar cells, J. Phys. Chem. Lett. 6 (2015) 3808-3814.

[43] E. Unger, E. Hoke, C. Bailie, W. Nguyen, A. Bowring, T. Heumüller, M. Christoforo, M. McGehee, Hysteresis and transient behavior in current–voltage measurements of hybrid-perovskite absorber solar cells, Energ. Environ. Sci. 7 (2014) 3690-3698.

[44] X. Zheng, B. Chen, C. Wu, S. Priya, Room temperature fabrication of CH 3 NH 3 PbBr 3 by anti-solvent assisted crystallization approach for perovskite solar cells with fast response and small J–V hysteresis, Nano Energy 17 (2015) 269-278.

[45] K. Wojciechowski, T. Leijtens, S. Spirova, C. Schlueter, M. Hoerantner, J.T.-W. Wang, C.-Z. Li, A.K.-Y. Jen, T.-L. Lee, H.J. Snaith, C_{60} as an efficient n-type compact layer in perovskite solar cells, J. Phys. Chem. Lett. 6 (2015) 2399-2405.

[46] Y. Zhang, M. Liu, G.E. Eperon, T.C. Leijtens, D. McMeekin, M. Saliba, W. Zhang, M. De Bastiani, A. Petrozza, L.M. Herz, Charge selective contacts, mobile ions and anomalous hysteresis in organic–inorganic perovskite solar cells, Mater. Horiz. 2 (2015) 315-322.

[47] J.H. Heo, M.S. You, M.H. Chang, W. Yin, T.K. Ahn, S.-J. Lee, S.-J. Sung, D.H. Kim, S.H. Im, Hysteresis-less mesoscopic $CH_3NH_3PbI_3$ perovskite hybrid solar cells by introduction of Li-treated TiO_2 electrode, Nano Energy 15 (2015) 530-539.

[48] M. Saliba, S.M. Wood, J.B. Patel, P.K. Nayak, J. Huang, J.A. Alexander-Webber, B. Wenger, S.D. Stranks, M.T. Hörantner, J.T.W. Wang, Structured organic–inorganic perovskite toward a distributed feedback laser, Adv. Mater. 23 (2015) 923-929.

[49] Z.-K. Tan, R.S. Moghaddam, M.L. Lai, P. Docampo, R. Higler, F. Deschler, M. Price, A. Sadhanala, L.M. Pazos, D. Credgington, Bright light-emitting diodes based on organometal halide perovskite, Nat. Nanotechnol. 9 (2014) 687-692.

[50] J. Wang, N. Wang, Y. Jin, J. Si, Z.K. Tan, H. Du, L. Cheng, X. Dai, S. Bai, H. He, Interfacial control toward efficient and Low-voltage perovskite light-emitting diodes, Adv. Mater. 27 (2015) 2311-2316.

[51] G. Li, Z.-K. Tan, D. Di, M.L. Lai, L. Jiang, J.H.-W. Lim, R.H. Friend, N.C. Greenham, Efficient light-emitting diodes based on nanocrystalline perovskite in a dielectric polymer matrix, Nano lett. 15 (2015) 2640-2644.

Supporting Information

Near-Neutral-Colored Semitransparent Perovskite Films Using a Combination of Colloidal Self-Assembly and Plasma Etching

Lijing Zhang,[a,b] Maximilian T. Hörantner,[c] Wei Zhang,[c,d] Qingfeng Yan,[b,*] Henry J. Snaith [c,*]

[a]School of Chemistry, Dalian University of Technology, Dalian, Liaoning, P. R. China.

[b]Department of Chemistry, Tsinghua University, Beijing 100084, China

[c]Department of Physics, University of Oxford, Clarendon Laboratory, Parks Road, Oxford, OX1 3PU, UK

[d]School of Chemistry, University of Lincoln, Joseph Banks Laboratories, Beevor Street, Lincoln LN6 7DL, UK

***Corresponding Authors:**

E-mail: yanqf@mail.tsinghua.edu.cn .

E-mail: h.snaith1@physics.ox.ac.uk

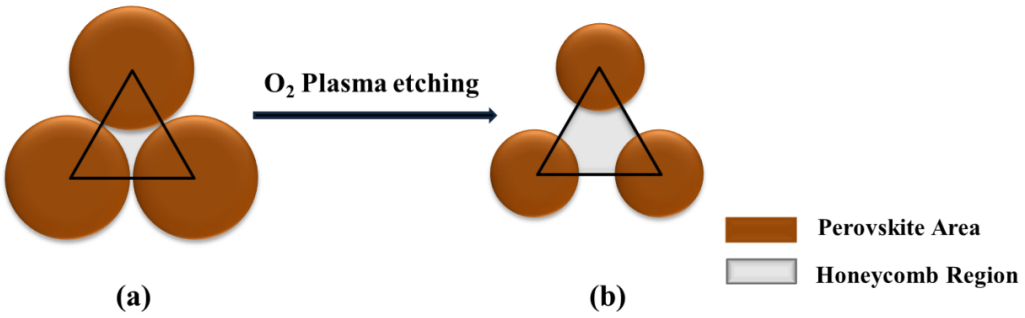

Fig. S1 Schematic depiction of the proportion change for honeycomb coverage before (a) and after (b) etching.

Theoretically, following a simple sphere model, the proportion of perovskite coverage can be calculated by the following equation:

$$\eta_{perovskite} = \frac{A_{perovskite}}{A_{triangle}} = \frac{\frac{1}{2}\pi r^2}{\frac{1}{2}\cdot 2R\cdot\sqrt{3}R} = \frac{\sqrt{3}\pi r^2}{6R^2} \quad (1)$$

Actually, the proportion of perovskite domains will be affected by various factors during the fabricating process, and will not cover the PS sphere space accurately. Thus, the coverage of inversed SiO_2 honeycomb structure was chosen to describe the ratio of transparent area. Correspondingly, the coverage proportion of SiO_2 honeycomb region is:

$$\eta_{SiO_2} = 1 - \eta_{perovskite} \quad (2)$$

Where the R is the diameter of the original colloid spheres and the r is the residual PS core's size. Thus the original $\eta^0_{perovskite}$ in theory is about 90.7%, the corresponding $\eta^0_{SiO_2}$ is 9.3%. For the PS cores array, the $\eta^t_{perovskite}$ is mainly determined by the original PS diameter (R) and the residual PS core's size (r). Here, the 600 nm PS colloidal monolayer was taken as an example. After etching for 8 min, the PS cores shrunk to 345 nm, according to Eq.(1) and (2), the $\eta^8_{perovskite}$ is about 30% and the $\eta^8_{SiO_2}$ is about 70%. Thus, we can obtain different η_{SiO_2} value by choosing PS spheres of different diameters or controlling the O_2 plasma etching time.

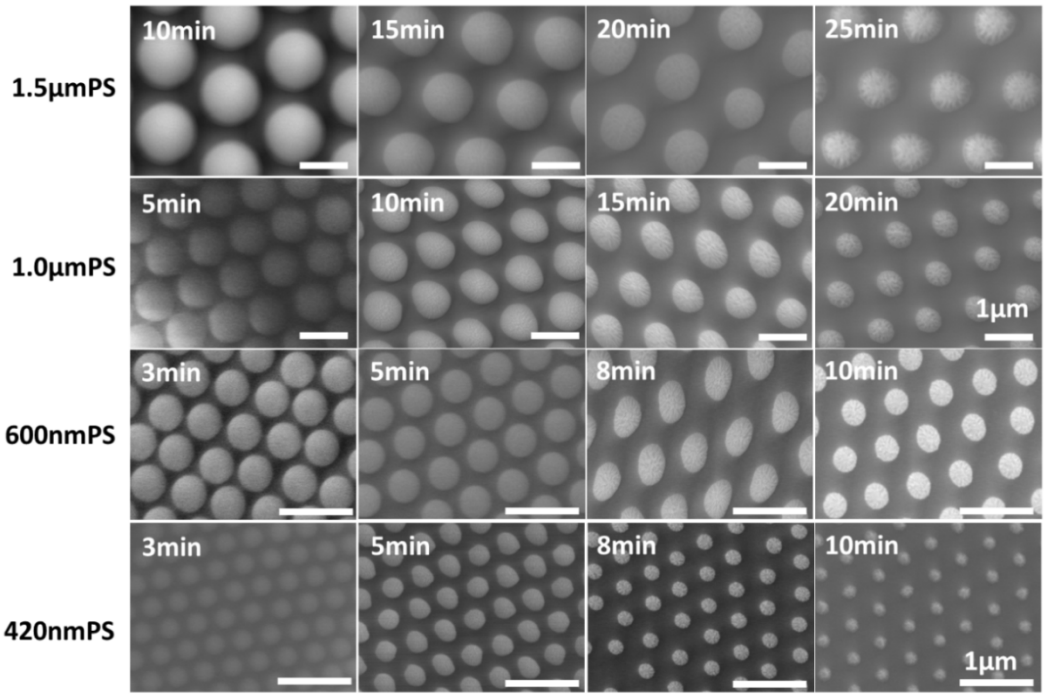

Fig. S2 SEM images of uniform PS core arrays generated by self-assembly of PS spheres with varied diameters and O_2 plasma etching time. The scale bar is 1μm.

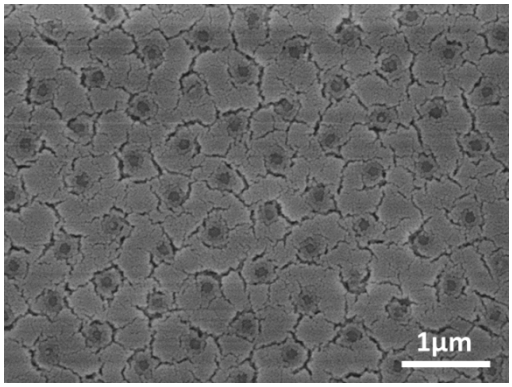

Fig. S3 SEM images of SiO_2 HC derived from 600 nm PS monolayer after O_2 plasma etching for 10 min, which showing series shallow pore arrays. The scale bar is 1μm.

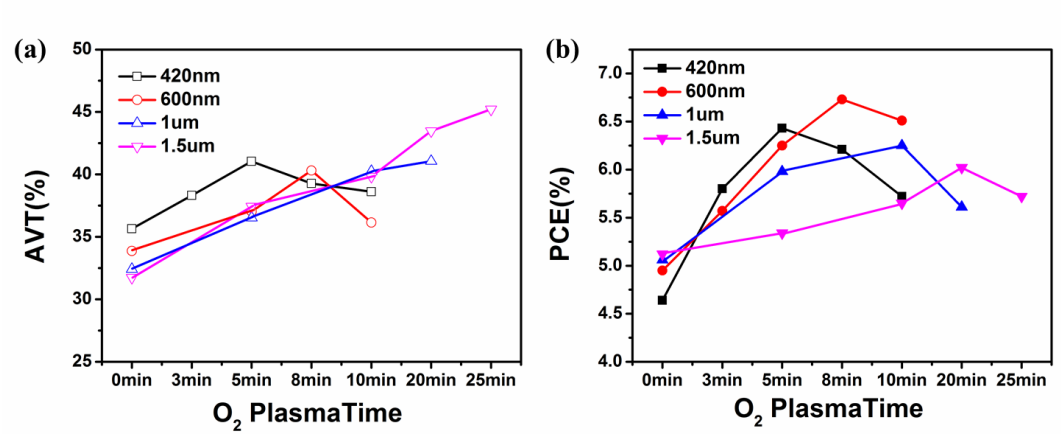

Fig. S4 The active layer AVTs (a) and device PCEs (b) of perovskite solar cells fabricated from PS CM templates with varied diameters of PS spheres and O_2 plasma etching time. The perovskite precursor concentration used here is 20 wt%.

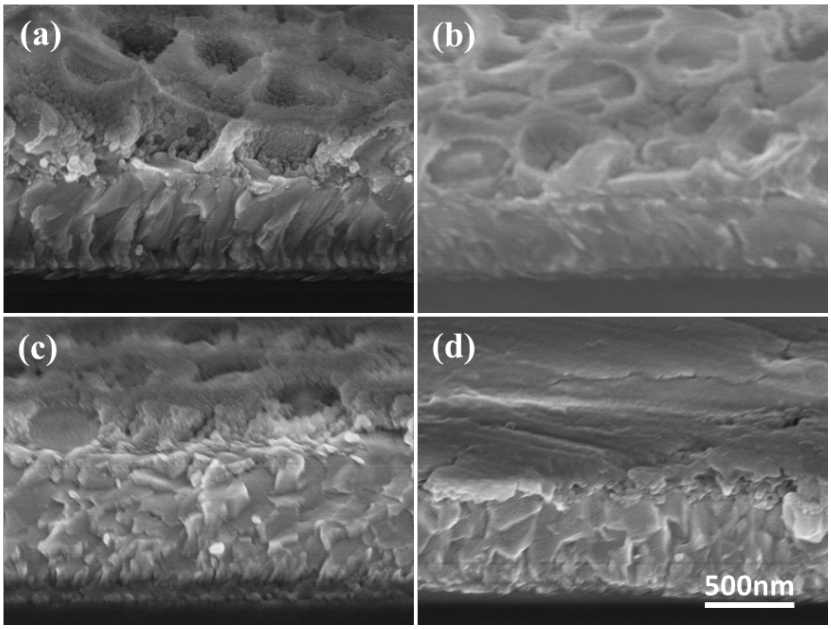

Fig. S5 Cross-sectional SEM images show the morphology of SiO_2 honeycomb structure patterned perovskite films derived from 600 nm-8 min etching PS core CMs. The used perovskite concentration is (a) 10 wt% (b) 20 wt%, (c) 30 wt% and (d) 40 wt%.

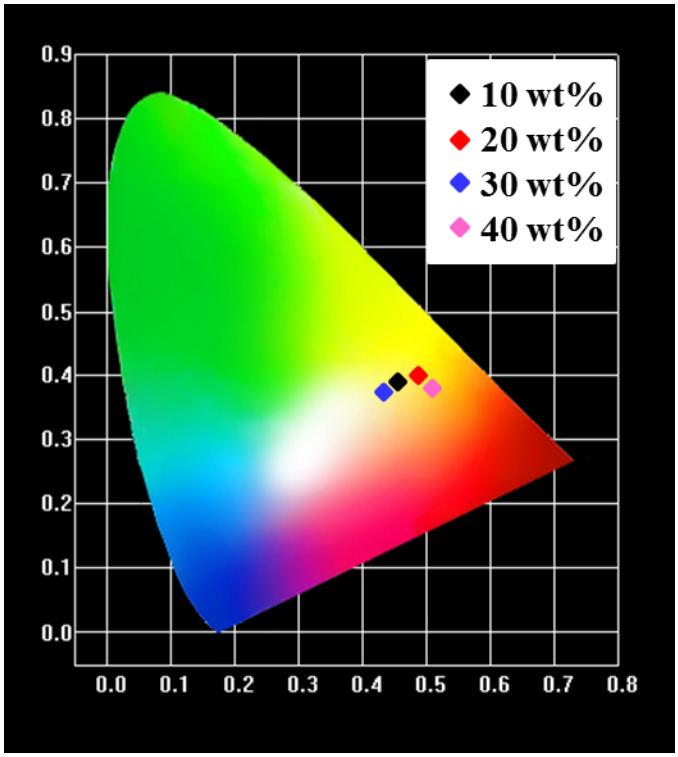

Fig. S6 Color coordinates on the CIE xy chromaticity diagram for the semitransparent perovskite films infiltrated from different precursor concentration.